IntraVital 3, e29728; July 2014; © 2014 Landes Bioscience

Comparison of intravital thinned skull and cranial window approaches to study CNS immunobiology in the mouse cortex

R Dixon Dorand[1], Deborah S Barkauskas[2], Teresa A Evans[3], Agne Petrosiute[4], Alex Y Huang[1,2,4,*]

[1]Department of Pathology; Case Western Reserve University School of Medicine; Cleveland, Ohio USA; [2]Department of Biomedical Engineering; Case Western Reserve University School of Medicine; Cleveland, Ohio USA; [3]Department of Neurosciences; Case Western Reserve University School of Medicine; Cleveland, Ohio USA; [4]Department of Pediatrics; Case Western Reserve University School of Medicine; Cleveland, Ohio USA

Keywords: Thinned skull, cranial window, two-photon, intravital microscopy, microglia, CNS imaging

Fluorescent imaging coupled with high-resolution femtosecond pulsed infrared lasers allows for interrogation of cellular interactions deeper in living tissues than ever imagined. Intravital imaging of the central nervous system (CNS) has provided insights into neuronal development, synaptic transmission, and even immune interactions. In this review we will discuss the two most common intravital approaches for studying the cerebral cortex in the live mouse brain for pre-clinical studies, the thinned skull and cranial window techniques, and focus on the advantages and drawbacks of each approach. In addition, we will discuss the use of neuronal physiologic parameters as determinants of successful surgical and imaging preparation.

Introduction

Two-photon laser scanning microscopy (2P-LSM)[1] allows for the visualization of fluorescently-tagged structures hundreds of microns deep within undisturbed living tissues. In addition, second harmonic generation by two photon excitation causes intrinsic emission of light energy under high-frequency pulse laser from ordered structures such as collagen and myosin without exogenous fluorescence probes, allowing for the observation of morphology in collagen-rich structures within tissues such as the lymph node and the brain.[2-4] While the field of immunology has taken advantage of two photon technology in the past decade,[5] neuroscientists first began using this technology in the late 1990s to monitor calcium flux in organotypic brain slice cultures.[6] Since 2005, intravital CNS imaging in the brain has flourished and scientists have captured biological processes including astrocyte reactivity, dendritic spine turnover, formation of plaques in Alzheimer disease, microglial dynamics, and immune cell trafficking.[7-13] A variety of techniques have been utilized to access the cortex, but the thinned skull and cranial window techniques to access the cortex dominate the literature. These two techniques are fundamentally different procedures with their own respective merits and drawbacks; therefore, choosing which imaging technique to employ for a given application is the first step to a successful experiment. Both techniques can lead to chronic inflammation, which induces the activation of microglia, the formation of scar tissue, changes of neuronal function and connections, and disruption of the neuropil with possible neuronal death. Therefore, careful consideration of both sterile technique and surgical expertise are paramount to a successful imaging experiment regardless of the approach taken. In this review we will discuss these two techniques, comparing and contrasting the pros and cons of each method.

*Correspondence to: Alex Y Huang; Email: alex.y.huang@case.edu
Submitted: 04/12/2014; Revised: 06/06/2014;
Accepted: 06/25/2014; Published Online: 07/07/2014
http://dx.doi.org/10.4161/intv.29728

Technical Considerations

Thinned Skull

Procedure

The thinned skull cranial window technique consists of thinning the calvarium to approximately 20 μm leaving an intact, almost transparent, periosteal layer. A dental drill is used to thin an area of 0.5 mm-1 mm in diameter to a total skull thickness of greater than 50 μm, completely removing the outer layer of compact bone and the majority of the inner layer of cancellous bone. A microsurgical blade is then used to shave an area of approximately 200 μm^2 in the remaining bone to a skull thickness of approximately 20 μm,[14] leaving the remaining bone intact to serve as structural support for the thinned area. Successful completion of the surgery maintains the integrity of the periosteum and peristoeal dura. Success can also be confirmed by checking for neurite blebbing via epi-fluoescent microscopy, if using reporter mice with neurons labeled with Thy-1,[15] or optically measuring skull thickness via confocal or 2P-LSM.[14] Despite minor bleeding from diploic vessels, thinned skull preparations leave the majority of anastomoses between the diploic vessels and dural vessels intact. Any minor bleeding should stop spontaneously within several seconds. The thinned skull technique leaves an imaging area with an average scanning diameter of 0.2 mm and a routine imaging depth of 250 μm, with the potential of imaging to a depth of 300–400 μm.[14,16] Once the surgical procedure is complete, the thinned skull preparation can be immediately

Table 1.

	Thinned Skull	Cranial Window
Depth of Surgery	Leave 20 - 30 μm of skull, keeping periosteum and dural-dipolic sinuses intact[14,78]	Completely remove the skull, dura mater intact[18,25,40,79]
Area of Window	0.2 - 2.0 mm[14,80]	2.0 - 5.0 mm[14,23]
Resting Period	None[14]	4–21 d depending on success of the preparation[15,27]
Imaging Depth	0 - 400 μm[14,16,23,40]	0 - 900 μm[14,23,24]
Number of Imaging Sessions	1 - 5[14,18]	Unlimited (until bone regrowth)[25,26]

imaged generating time points from one minute to five days post-op.[14] After five days, skull regrowth occludes the preparation and necessitates removal of excess bone deposition. The skull can be re-thinned at any time point up to five times, providing total imaging period from days to years (**Table 1**).[14]

Limitations

The greatest limitation to the thin skull preparation is surgical skill since the thinning procedure provides an opportunity for mechanical stress to disrupt the underlying CNS. Thinning the skull is a balance between access to the CNS and damage due to mechanical instability. Some reports claim that 30 μm thickness provides access to fluorescent signal in the brain parenchyma without interference or spherical abberation.[17] However, other reports urge that the preparation must be no thicker than 25 μm for optimal imaging and no less than 20 μm to avoid neuronal blebbing or microglia and astrocyte activation.[14] In agreement with this, other reports argue that although thinning the bone to 5μm (**Fig. 1A-C**) may provide higher imaging resolution at early time points as compared with areas with 20-μm thickness (**Fig. 1D-F**), the probability of mechanical disruption of CNS structures increases due to lack of structural integrity in the excessively thinned skull. In addition, thinned skull preparations can also be difficult to perform. The curvature of the skull can make thinning to a specific depth over a large area technically challenging, resulting in varying thickness of the skull. As is emphasized in the supplemental methods of Xu et al., if the preparation is thinned to 15 μm at any point, that area can be no more than 0.3 mm in diameter to avoid damage to the underlying tissue.[15] Repeated thinning of the skull also results in additional opportunity for trauma. There are varying reports of window failure in the literature, including one study reporting that their thinned skull preparations become opaque on the first day after thinning, thus limiting the initial imaging time from 5 d to 24 h.[18] Due to mechanical stress on the underlying vasculature, bleeding is common at the site of drilling and can be excessive at times.[18] Disruption of other underlying structures is possible, although this can be minimized with proper surgical technique.

Variations

The polished and reinforced thinned skull procedure (PoRTS) consists of thinning an area of 0.7 – 1.0 mm to 10–15 μm thickness, polishing the remaining tissue with grit suspended in artificial cerebrospinal fluid (aCSF), and placing a cover glass over the thinned area.[16] PoRTS allows for imaging to a depth of 250 μm without altering microvasculature for 40 d.[16] Furthermore, this technique quells astrocyte activation as indicated by a decrease in glial fibrillary acidic protein (GFAP) staining and a decrease in microglial activation based identification of microglial morphology in $CX_3CR1^{+/GFP}$ transgenic mice. The major drawback to the PoRTS system is a loss in optical resolution.[16] This is due to the presence of glass in addition to the bone through which the laser must penetrate and signals are detected.

Cranial Window

Procedure

The cranial window technique also consists of grinding down the calvarium to a transparent layer along the edges of the intended craniotomy before removing the bone to create a small full craniotomy. Rather than making a 0.2 mm thinned area, the bone is ground down around the perimeter of a 3 mm[18] circle creating a flap or island of bone that can be carefully removed using a pair of fine forceps.[19] While diploic vessels may bleed during thinning of the bone the bleeding usually ceases spontaneously within a few seconds. After removing the flap of bone, the exposed dura is bathed in either a saline solution or aCSF. Additionally, a piece of gelatin surgical foam, soaked in the solution of choice, is placed upon the exposed tissue to quell bleeding and maintain tissue moisture.[20] After drying the skull around the window, a round cover glass is placed on top of the dura and sealed using cyanoacrylate glue. In addition, some protocols call for a layer of 1.2% low melting temperature agarose on top of the dura[19,21,22] to help reduce movement of the underlying tissue.[18] Lastly, dental acrylic is placed around the window and edges of the exposed tissue in order to stabilize the glass cover as well as provide a reservoir for holding fluid for immersion objectives. Successful completion of the surgery is initially determined by absence of blood or air pockets beneath the implanted window.[18,20] Depending on the success of the preparation, the brain can be imaged through the window to a depth of 0–900 μm as long as any underlying inflammation or opacity has subsided.[15,23,24] After the initial 4 d to 2 wk of recovery time, the window can be imaged at any time point from several weeks to several months depending on bone regrowth and window occlusion.[14,25-27] **Table 1** summarizes the major differences in imaging parameters and surgical procedures between the thinned skull and cranial window approaches.

Limitations

As with the thinned skull technique, the most challenging aspect of a cranial window preparation is the surgical and technical skill required for a successful preparation. While it is not

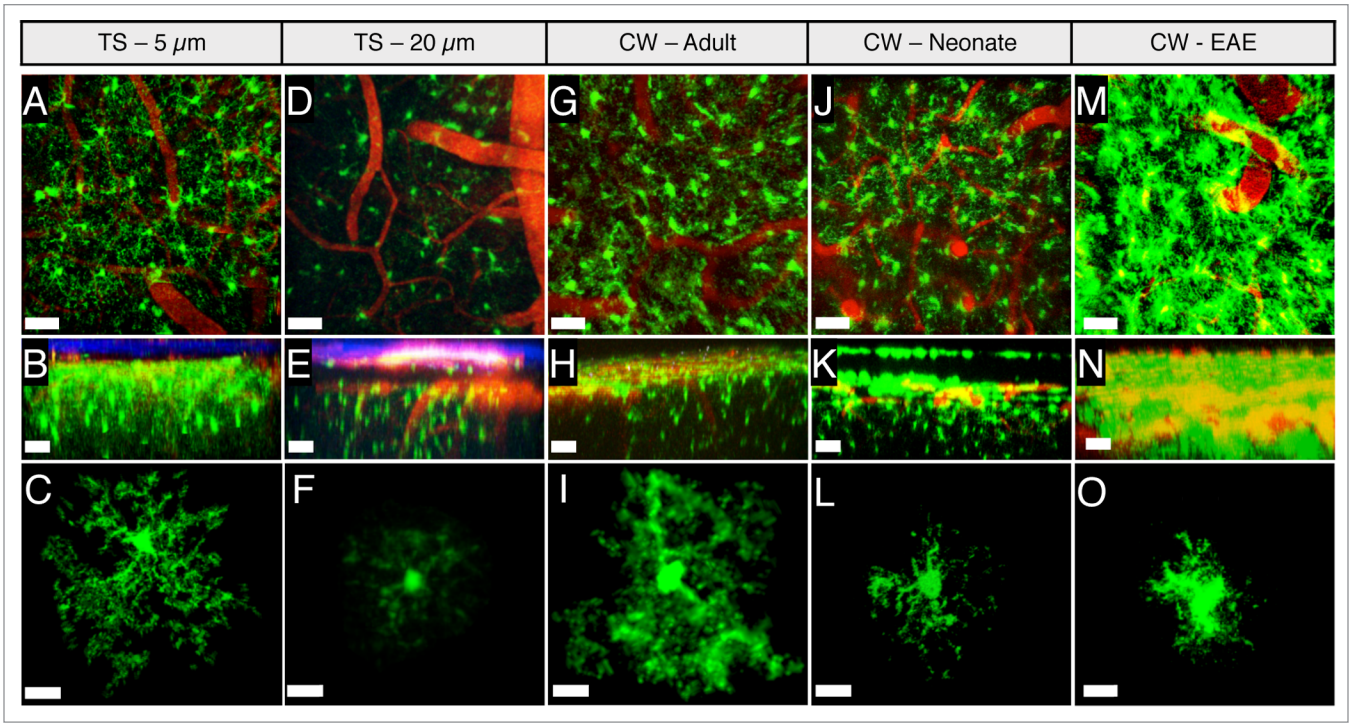

Figure 1. Comparison of microglia morphology using thinned skull and cranial window approaches. 2P-LSM was used to capture images within the CNS of CX3CR1$^{+/GFP}$ mice. The cranial bone was thinned (TS) to either 5 μm (A-C) or 20 μm (D-F) and imaged immediately using a Leica SP5 fitted with a DM6000 stage and a 16W Ti/Sapphire IR laser (Chameleon, Coherent) through a 20x water immersion objective (NA: 1.0). Alternatively, cranial windows (CW) were implanted on adult (G-I; M-O) and day 10 neonatal mice (J-L). Adult animals were given 7 d and neonates were given 4 d to rest after CW implantation prior to imaging. (M-O) Mice underwent EAE induction as previously described.[77] All images were collected at a resolution of 1024x1024 between 2–5 μm z-intervals. Vessels were highlighted with 150 kD TRITC dextran. The fluorescent imaging data were analyzed using Imaris (Bitplane, Inc.). **(A,D,G,J)** The xy axis demonstrates the normal, uniform distribution of microglia throughout the parenchyma. Scale bar = 40 μm. **(M)** Accumulation of microglia on day 5 after EAE induction. Note the difference of detectable microglia projections between preparations. Scale bar = 40 μm. **(B,E,H,K,N)** Same images as above in the xz dimension, demonstrating the imaging depth for each preparation. Scale bar = 40 μm. **(B,E)** Blue second harmonic signals show the intact bone. (**C,F,I,L,O**) Zoomed-in view of the cell body and projections of individual microglia. Scale bar = 15 μm. **(C,F,I,L)** In the homeostatic CNS, microglia projections emanate in all directions. The size of microglia cell body range from a maximum diameter of 7.5–15 μm. **(O)** In EAE, microglia shorten their projections and assume an amoeboid shape with an increased cell body size.

necessary to measure the depth of the cranial thinning around the perimeter of the craniotomy, it is still possible to drill through the inner layer of compact bone and potentially disrupt the dura mater and underlying CNS tissue while creating the craniotomy. Additionally, when removing the bone flap, the forceps should be as close to parallel as possible to avoid mechanical injury as the dura can be attached to the overlying bone. Lastly, the dental acrylic must be applied in as smooth a layer as possible to avoid removal of the cranial window by the animal post implantation. Physiologically, fibrotic scaring or periosteal dura and bone regrowth can occlude the window over time, eliminating the possibility of further imaging.[18] In addition, any damage to the vessels in the dura during the surgical procedure can form pools of coagulated blood under the window's surface, once again ending the possibility of imaging. Successful completion of the window implantation, defined by optical clarity at the time of imaging (i.e., no bone regrowth, scarring, or overt inflammation), varies greatly with skill. Success rates vary from 30–80%.[15,18]

Variations

One variation on the cranial window technique is implantation of windows in neonates.[20,21,28,29] Utilizing modifications to the protocol described above, researchers have been able to image developing neurons in mouse pups as young as day 5 after birth by covering the intact dura with 1.2% low melting temperature agarose before adding the glass window to ensure image clarity and prevent bone regrowth.[21] In another preparation, a ring of cyanoacrylate glue was applied around the area of the coverslip before drilling and bone flap removal to ensure structural integrity of the areas around the flap, taking care not to cross suture lines to allow growth of the developing skull.[20] Even so, windows placed on P5 pups have only been imaged for a few days due to failure of the animals to thrive. However, pups with windows implanted at day 8 after birth have not shown signs of weight loss, altered neuronal branching density or vessel formation in the dura and do not require the use of agarose underneath the glass.[20] Another variation on the cranial window is the addition of 2P-LSM fiberscopes to allow imaging of freely moving animals. This setup can be added to an existing 2P-LSM system but needs sufficient power to overcome the dispersions and power loss generated when imaging through the fiberscope.[30] In addition, placement of the fiberscope deep in the hippocampus involves extensive CNS tissue disruption as compared with either

thinned skull or cranial window approaches, although it allows imaging of deeper structures.[31] Another variation is the addition of a miniature scanning device, which allows for imaging of the animal while it is moving around a cage normally,[30] although this is not widely available.

The Great Debate: Neuronal Kinetics and Glial Activation

Dendritic Spine Turnover

Dendritic spines are protrusions from dendrites often characterized by a thin neck and bulbous end.[32] Spines contain postsynaptic structures, and spine density is often used as a proxy for synapse number. While the precise molecular mechanisms for the formation of dendritic spines remain unclear, it has been hypothesized that dendritic filopodia, often described in imaging studies, are immature spines.[32] The number of filopodia decreases from 10% of total protrusions at P30 to 2–3% in adult animals, indicating a possible role in development.[33] Rates of dendritic spine turnover also vary drastically with the age of the animals, with 27% spine turn over in young animals vs. 4% in adult animals over the course of a month.[34] Another physiologic parameter is the anatomic location of imaged spines within different cortical layers. Because 2P-LSM can potentially reach a depth of 400–900 μm, all cortical layers can theoretically be imaged. Lee et al. utilized cranial windows to report that more spine remodeling occurs at the limits of the dendritic arbor in layer 2/3 than in either layer 1 or deeper layers, correlating spine turnover to cortical circuit formation in a layer dependent pattern.[35]

Proponents of thinned skull preparations often point to differences in dendritic spine and filopodia turnover rates as evidence of altered neuronal kinetics caused by chronic window implantation. However, the age of the experimental animals, imaging locale, and model system must be considered for each comparative experiment. Additionally, because there is no current consensus for the mathematical quantification of turnover rate when comparing experiments between labs, scoring criteria varies for identification of spine formation and dissolution.[18] However, in many studies, rates of dendritic spine turnover do differ significantly when comparing thinned skull and open window preparations.[15,22,36,37] Compared with thinned skull, Xu et al. found that dendritic spine turnover in cortical layer I from pyramidal neurons was significantly higher using cranial windows in Thy-1 YFP H line over the course of a month.[15] Even allowing mice two weeks to recover after window implantation, cranial window preparations resulted in 24.7% of spines turned over in two weeks and 34.3% over 1 mo compared with 4.9% over in two weeks and 6.4% turnover in one month with the thinned skull technique.[15] Allowing a four to five week rest period for the cranial window allows for spine turnover rates that begin to approach that in the thinned skull preparations. Brown et al. showed a dendritic spine turnover rate of 8.8% per week with 4.6% of spines formed and 4.2% lost after the longer rest period.[36] However, the four to five week rest period may limit certain experimental designs. To address this issue Keck et al. demonstrated that spine turnover over the course of one week was similar after allowing the animals to rest for either two weeks and ten weeks post window implantation in the Thy-1 GFP M line.[38] Last, Holtmaat et al. showed that clear window preparations 2 wk post-surgery in Thy-1 GFP M line had minimal change in spine turnover over the course of the subsequent 3 mo,[18] indicating that the particular duration of rest may not directly affect turnover. Although all of these results may not be directly comparable to the more commonly used Thy-1 YFP H line due to different labeled neuronal populations,[39] they suggest that the resting time can be shortened when the window implantation is performed by a skilled surgeon.

These results clearly illustrate the variability in spine turnover results with window preparations based on operator, laboratory and mouse line. Surgical technique is an important first part of this variability. The initial study by Xu reported that 30% of mice maintained non-opaque windows that could be utilized for 2P-LSM.[15] This contrasts with reports from other labs, including our own, with a success rate of 70–80%.[18] Second, the multiple neuronal fluorescent reporter mouse lines resulted in different neuronal populations used for analysis in these studies, making them difficult to compare.[39] Differences in resolution at varying imaging depths may also explain variations in results, although Isshiki and Okabe found that at a depth of 50 μm the point spread function of 2P-LSM was comparable between preparations. Differences in access may also affect results when imaging to greater depths; the cranial widow technique resulted in better image resolution and theoretically recognition of fine neuronal structures such as spines.[40] The discrepancy in resolution could account for the differences in spine and filopodia turnover previously discussed because these microstructures require optimal resolution for quantification.

Glial Activation

The cytokine profile of the normal interstitial fluid in the CNS consists of TGF-β, PGE2, and other mediators that maintain the CNS in a non-inflamed state.[41] Supportive structures within the brain rapidly respond to any changes in inflammatory mediators, ischemia, changes in neuronal activity, trauma or other sign of damage.[42,43] As described earlier, surgical preparations for imaging access can cause inflammation from surgical trauma due to mechanical disruption of brain parenchymal and meningeal structures, or introduction of foreign particles or pathogens.[15,18,44] Activation of inflammatory cells in the glial limitans can also lead to changes in the blood brain barrier, resulting in further inflammatory changes. Several groups have shown differential activation of astrocytes and microglia both within the glia limitans and the parenchyma under thinned skull vs. cranial window preparations.[9,10,15,18,36,45] Evidence of reactive gliosis can be used as an indicator of damage to the CNS parenchyma or inflammation and can complicate the study of many disease models.[42,46] With tissue injury, glial cells including astrocytes, microglia, oligodendrocytes, and glial precursor cells are some of the first to respond, forming a scar termed reactive gliosis. The glial scar may help to maintain CNS integrity after an injury and prevent increases in injury size, although it can also inhibit the regrowth of neurons through the same area.[47,48] Here, we briefly describe parameters of astrocytes and microglia activation and

markers that are routinely used to assess the physiological consequences of different intravital approaches.

Astrocyte Activation

During homeostasis, adult CNS astrocytes have a characteristic bushy appearance consisting of thin processes that form a web encompassing the entire CNS and react by changing protein levels and morphology when CNS damage occurs.[42,47,49] GFAP, a member of the intermediary filament proteins, is upregulated during activation.[49] GFAP, along with vimentin, nestin, and synemin can form filaments within astrocytes alone or in concert with each other when the cell is activated.[50,51] The expression of more than one of these proteins is required for complete filament formation under pathologic conditions.[50] Additionally, hypertrophy of astrocytic processes is another hallmark of reactive astrocytes that is closely tied to the expression of the intermediary filament proteins.[52] These cells can be identified in tissues by staining with anti-GFAP antibody, or in animals expressing fluorescent proteins under the GFAP promoter.[51,53-55] These activated astrocytes are a component of a stiff scar over the injured tissue, playing a dual role in minimizing damage after an insult and playing a role in the healing process. When imaging through a cranial window or thinned skull, the presence of the scar can often be a useful indicator of damage to the brain parenchyma incurred during surgery.

Microglia Activation

Microglia are the innate immune cells of the CNS and react immediately and dramatically to inflammatory processes within the brain.[41] Through a thinned skull approach, microglia have been described in the resting state as highly dynamic, extending their processes several microns and changing their branching patterns while maintaining a constant number of branches (**Fig. 1A-L**).[10,11] Activated microglia are routinely identified by changes in cell shape, cell body size, IBA-1 and CD68 expression.[56,57] A quiescent microglia changes from its resting state to an activated state via a process involving retraction of processes, thickening of processes, and enlargement of the cell body. At the end of this transition, the cell takes on an amoeboid morphology indistinguishable from a macrophage.[43,57] Using the thinned skull approach, extensive branching patterns of individual microglia can be clearly reconstructed with the assistance of imaging software (**Fig. 1C, F**). Basic measurements such as cell body size and gross morphology are similar in both thinned skull preparations, although the optical resolution of 5 μm thinned skull preparations (**Fig. 1C**) is superior to that of 20 μm thinned skull preparations (**Fig. 1F**), as evidenced by number and fluorescence intensity of branches detected. Additionally, cranial window preparations (**Fig. 1I and L**) of quiescent microglia show similar morphology to those imaged through uninjured acute 5 μm thinned skull preparations, and the image quality is superior to 20 μm thinned skull preparations. When EAE is induced in animals equipped with cranial windows (**Fig. 1M-O**), the changes associated with individual microglia morphology (**Fig. 1O**) are striking when compared with their quiescent counterparts with the same window preparation (**Fig. 1C, F, I, and L**). These changes are comparable to those described with general microglial activation in states of injury or stress.[43]

More recently, the $CX_3CR1^{GFP/+}$ reporter mouse has been employed for intravital CNS imaging to identify microglia for morphological studies.[58] In one of the original reports of in vivo microglial physiology, microglia labeled in this manner extended processes toward a laser burn forming bulbous ends without movement of or changes to their cell bodies.[10,11] A later study demonstrated the morphologic changes from resting, ramified microglia to activated microglia.[59] A more recent study showed robust microglial activation as defined by cellular accumulation and morphological changes during CNS neuroinflammation (**Fig. 1M-O**).[60]

Complicating the use of microglial morphology to assess window integrity is the activation of microglia and lack of ramification in response to other insults such as stress from restraint. Hyper-ramification of secondary branches and process extension by microglia have been observed in response to chronic restraint stress, with a 21% increase in microglial branching between 8 and 28 μm from the soma in stressed animals.[61] However, increased ramification was not accompanied by increased expression of microglial activation makers such MHC-II, CD68, Caspase-3, or IL-1β.[43,61-64,]

Comparative Studies

The roles of activated astrocytes and microglia in reactive gliosis are still under investigation.[51] However, markers of glial activation can be used to evaluate the effectiveness of experimental techniques. Utilizing $CX_3CR1^{+/GFP}$ and IBA-1 to identify microglial morphology, Xu et al. showed extensive activation of microglia in cranial window preparations based on process orientation and density.[15] Evaluating astrocyte staining in their study of dendritic spine turnover, Brown et al. found that astrocytes were not activated and did not express GFAP after four to five weeks following cranial window surgery.[36] However, critical evaluation of the GFAP staining presented in both Brown and Xu shows an absence of resting $GFAP^+$ astrocytes in contrast with other reports that show that resting astrocytes express a baseline level of GFAP, which is upregulated upon activation.[51,53,54]

Some striking examples of differences between thinned skull and window preparations came from studies of plaque formation in Alzheimer Disease (AD). Yan et al. showed differential outcomes of amyloid plaque formation in the APP/PS1 mouse model by comparing thinned skull vs. cranial window techniques. They tracked Aβ plaque development over a course of 3 mo, finding that Aβ plaque size increased more reliably in younger (6 mo) mice as compared with older (10 mo) mice. Interestingly, smaller plaques grew rapidly to form large plaques only in thinned skull preparations, and the investigators hypothesized that the glial activation underneath the window preparation was responsible for preventing plaque formation.[9] However, several considerations should be made before dismissing the use of cranial windows. First, this study did not show evidence of GFAP staining in resting astrocytes as would be expected. In addition, Iba-1 staining did not reveal an overt increase in cell size or change in microglial process morphology in mice implanted with the windows. Furthermore, despite the fact that their role in plaque clearance has not been definitively characterized, activated microglia have a significantly larger soma and accumulate around amyloid plaques in AD in

vivo,[65,66] which was not seen in this case. Second, considering the size of plaques at the start of the study, it is conceivable that the plaques did not grow in size in the mice with the cranial windows since the plaques were already large at the beginning of the imaging experiment. Lastly, in window preparations utilizing Tg2576 mice, Burgold et al. were able to show that plaques grew in both 12 and 18 mo old mice, and that new plaques grew faster than pre-existing ones. They also observed that a 21 d resting period was sufficient to reduce experimental variation induced by open craniotomy,[45] arguing that an adequate rest period post-surgery is sufficient to overcome experimental variation in cranial imaging techniques.

Conclusion

When evaluating options for intravital CNS imaging, there are several factors to consider. First, the choice of technique should reflect the experimental design, i.e., thinned skull technique is a good method for either acute imaging or imaging only a few time points. For an experiment that requires longitudinal and frequent imaging, the cranial window provides a stable, long-term imaging solution. Second, and perhaps more importantly when coupled with 2P-LSM, imaging depth is another important factor to consider. As demonstrated by Isshiki and Okabe, the point spread function of thinned skull imaging decreases after 50 μm making it hard to distinguish fine neuronal structures such as dendritic spines and filipodia,[40] while the cranial window preparation does not have this issue. Therefore, cranial windows are preferred when imaging deep or when imaging fine morphological structures. Third, if a cranial window is chosen as the approach of choice, a resting period of 1–3 wk is preferable before collecting experimental results in the adult. Shorter resting periods have been accepted in neonates due to successful imaging in animals up to one day after window implantation.[20,21,29,67,68] Available studies comparing thinned skull and rested cranial windows demonstrate that, given adequate time, reactive astrocytes and microglia will regain their resting phenotype even if activated previously. Surgical trauma or introduction of contaminants through the skin or bone marrow vasculature can happen with either approach and lead to systemic and local inflammatory responses. Waiting 1–3 wk after window implantation prior to imaging may also help minimize local and systemic host responses toward potential contaminants introduced during the surgical procedure.[69] The duration of the resting period depends on the skill of the surgeon, as the success of preparations is highly variable among laboratories and individual researchers. While this review focuses on two different technical approaches to image the mouse cortex, many of the principles, considerations, and caveats outlined in the above discussions are generally applicable to intravital imaging approaches in other anatomical sites including the spine.[70-76] Each experimental approach and anatomical site presents its unique set of challenges, such that proper design, execution and interpretation of experiments really rest on the skill of the surgeon, the experimental design, and proper experimental controls. Ultimately, successful intravital CNS imaging begins with the age-old tenant: a steady set of hands is paramount to experimental designs or interpretation of results.

Acknowledgments

The following agencies provided funding support for this study: MSTP T32 GM007250 (RDD and TAE); 5T32EB7509 (DSB); The Wolstein Pediatric Cancer Research Fund (RDD); 5K12HD057581 (AP); Dana Foundation (AYH), St. Baldrick's Foundation (AYH and AP), Hyundai Hope-on-Wheel's Program (AYH and AP), Gabrielle's Angel Foundation (AYH), Alex's Lemonade Stand Foundation (AYH), and NCI R01 CA154656 (AYH).

Authorship Contribution

RDD, DSB, TAE, AP and AYH contributed to researching and writing the manuscript.

References

1. Denk W, Strickler JH, Webb WW. Two-photon laser scanning fluorescence microscopy. Science 1990; 248:73-6; PMID:2321027; http://dx.doi.org/10.1126/science.2321027
2. Kawakami N, Flügel A. Knocking at the brain's door: intravital two-photon imaging of autoreactive T cell interactions with CNS structures. Semin Immunopathol 2010; 32:275-87; PMID:20623286; http://dx.doi.org/10.1007/s00281-010-0216-x
3. Williams RM, Zipfel WR, Webb WW. Interpreting second-harmonic generation images of collagen I fibrils. Biophys J 2005; 88:1377-86; PMID:15533922; http://dx.doi.org/10.1529/biophysj.104.047308
4. Campagnola PJ, Millard AC, Terasaki M, Hoppe PE, Malone CJ, Mohler WA. Three-dimensional high-resolution second-harmonic generation imaging of endogenous structural proteins in biological tissues. Biophys J 2002; 82:493-508; PMID:11751336; http://dx.doi.org/10.1016/S0006-3495(02)75414-3
5. Germain RN, Robey EA, Cahalan MD. A decade of imaging cellular motility and interaction dynamics in the immune system. Science 2012; 336:1676-81; PMID:22745423; http://dx.doi.org/10.1126/science.1221063
6. Yuste R, Denk W. Dendritic spines as basic functional units of neuronal integration. Nature 1995; 375:682-4; PMID:7791901; http://dx.doi.org/10.1038/375682a0
7. Risher WC, Andrew RD, Kirov SA. Real-time passive volume responses of astrocytes to acute osmotic and ischemic stress in cortical slices and in vivo revealed by two-photon microscopy. Glia 2009; 57:207-21; PMID:18720409; http://dx.doi.org/10.1002/glia.20747
8. Zuo Y, Yang G, Kwon E, Gan W-B. Long-term sensory deprivation prevents dendritic spine loss in primary somatosensory cortex. Nature 2005; 436:261-5; PMID:16015331; http://dx.doi.org/10.1038/nature03715
9. Yan P, Bero AW, Cirrito JR, Xiao Q, Hu X, Wang Y, Gonzales E, Holtzman DM, Lee J-M. Characterizing the appearance and growth of amyloid plaques in APP/PS1 mice. J Neurosci 2009; 29:10706-14; PMID:19710322; http://dx.doi.org/10.1523/JNEUROSCI.2637-09.2009
10. Davalos D, Grutzendler J, Yang G, Kim JV, Zuo Y, Jung S, Littman DR, Dustin ML, Gan W-B. ATP mediates rapid microglial response to local brain injury in vivo. Nat Neurosci 2005; 8:752-8; PMID:15895084; http://dx.doi.org/10.1038/nn1472
11. Nimmerjahn A, Kirchhoff F, Helmchen F. Resting microglial cells are highly dynamic surveillants of brain parenchyma in vivo. Science 2005; 308:1314-8; PMID:15831717; http://dx.doi.org/10.1126/science.1110647
12. Kawakami N, Nägerl UV, Odoardi F, Bonhoeffer T, Wekerle H, Flügel A. Live imaging of effector cell trafficking and autoantigen recognition within the unfolding autoimmune encephalomyelitis lesion. J Exp Med 2005; 201:1805-14; PMID:15939794; http://dx.doi.org/10.1084/jem.20050011
13. Fumagalli S, Coles JA, Ejlerskov P, Ortolano F, Bushell TJ, Brewer JM, De Simoni MG, Dever G, Garside P, Maffia P, et al. In vivo real-time multiphoton imaging of T lymphocytes in the mouse brain after experimental stroke. Stroke 2011; 42:1429-36; PMID:21441145; http://dx.doi.org/10.1161/STROKEAHA.110.603704

14. Yang G, Pan F, Parkhurst CN, Grutzendler J, Gan W-B. Thinned-skull cranial window technique for long-term imaging of the cortex in live mice. Nat Protoc 2010; 5:201-8; PMID:20134419; http://dx.doi.org/10.1038/nprot.2009.222
15. Xu H-T, Pan F, Yang G, Gan W-B. Choice of cranial window type for in vivo imaging affects dendritic spine turnover in the cortex. Nat Neurosci 2007; 10:549-51; PMID:17417634; http://dx.doi.org/10.1038/nn1883
16. Drew PJ, Shih AY, Driscoll JD, Knutsen PM, Blinder P, Davalos D, Akassoglou K, Tsai PS, Kleinfeld D. Chronic optical access through a polished and reinforced thinned skull. Nat Methods 2010; 7:981-4; PMID:20966916; http://dx.doi.org/10.1038/nmeth.1530
17. Nayak D, Zinselmeyer BH, Corps KN, McGavern DB. In vivo dynamics of innate immune sentinels in the CNS. Intravital 2012; 1:95-106; PMID:24078900; http://dx.doi.org/10.4161/intv.22823
18. Holtmaat A, Bonhoeffer T, Chow DK, Chuckowree J, De Paola V, Hofer SB, Hübener M, Keck T, Knott G, Lee W-CA, et al. Long-term, high-resolution imaging in the mouse neocortex through a chronic cranial window. Nat Protoc 2009; 4:1128-44; PMID:19617885; http://dx.doi.org/10.1038/nprot.2009.89
19. Svoboda K, Denk W, Kleinfeld D, Tank DW. In vivo dendritic calcium dynamics in neocortical pyramidal neurons. Nature 1997; 385:161-5; PMID:8990119; http://dx.doi.org/10.1038/385161a0
20. Cruz-Martin A, Portera-Cailliau C. In vivo imaging of axonal and dendritic structures in neonatal mouse cortex. Cold Spring Harb Protoc 2014; 2014:57-64; PMID:24371322; http://dx.doi.org/10.1101/pdb.prot080150
21. Portera-Cailliau C, Weimer RM, De Paola V, Caroni P, Svoboda K. Diverse modes of axon elaboration in the developing neocortex. PLoS Biol 2005; 3:e272; PMID:16026180; http://dx.doi.org/10.1371/journal.pbio.0030272
22. Holtmaat AJGD, Trachtenberg JT, Wilbrecht L, Shepherd GM, Zhang X, Knott GW, Svoboda K. Transient and persistent dendritic spines in the neocortex in vivo. Neuron 2005; 45:279-91; PMID:15664179; http://dx.doi.org/10.1016/j.neuron.2005.01.003
23. Shih AY, Driscoll JD, Drew PJ, Nishimura N, Schaffer CB, Kleinfeld D. Two-photon microscopy as a tool to study blood flow and neurovascular coupling in the rodent brain. J Cereb Blood Flow Metab 2012; 32:1277-309; PMID:22293983; http://dx.doi.org/10.1038/jcbfm.2011.196
24. Lathia JD, Gallagher J, Myers JT, Li M, Vasanji A, McLendon RE, Hjelmeland AB, Huang AY, Rich JN. Direct in vivo evidence for tumor propagation by glioblastoma cancer stem cells. PLoS One 2011; 6:e24807; PMID:21961046; http://dx.doi.org/10.1371/journal.pone.0024807
25. De Paola V, Holtmaat A, Knott G, Song S, Wilbrecht L, Caroni P, Svoboda K. Cell type-specific structural plasticity of axonal branches and boutons in the adult neocortex. Neuron 2006; 49:861-75; PMID:16543134; http://dx.doi.org/10.1016/j.neuron.2006.02.017
26. Lee W-CA, Huang H, Feng G, Sanes JR, Brown EN, So PT, Nedivi E. Dynamic Remodeling of Dendritic Arbors in GABAergic Interneurons of Adult Visual Cortex. PLoS Biol [Internet] 2006 [cited 2014 Jan 22]; 4. Available from: http://www.ncbi.nlm.nih.gov/pmc/articles/PMC1318477/
27. Barkauskas DS, Evans TA, Myers J, Petrosiute A, Silver J, Huang AY. Extravascular CX3CR1+ cells extend intravascular dendritic processes into intact central nervous system vessel lumen. Microsc Microanal 2013; 19:778-90; PMID:23642852; http://dx.doi.org/10.1017/S1431927613000482
28. Cane M, Maco B, Knott G, Holtmaat A. The relationship between PSD-95 clustering and spine stability in vivo. J Neurosci 2014; 34:2075-86; PMID:24501349; http://dx.doi.org/10.1523/JNEUROSCI.3353-13.2014
29. Gray NW, Weimer RM, Bureau I, Svoboda K. Rapid Redistribution of Synaptic PSD-95 in the Neocortex In Vivo. PLoS Biol [Internet] 2006 [cited 2014 Jan 22]; 4. Available from: http://www.ncbi.nlm.nih.gov/pmc/articles/PMC1634879/
30. Helmchen F, Denk W, Kerr JND. Miniaturization of two-photon microscopy for imaging in freely moving animals. Cold Spring Harb Protoc 2013; 2013:904-13; PMID:24086055; http://dx.doi.org/10.1101/pdb.top078147
31. Barretto RPJ, Ko TH, Jung JC, Wang TJ, Capps G, Waters AC, Ziv Y, Attardo A, Recht L, Schnitzer MJ. Time-lapse imaging of disease progression in deep brain areas using fluorescence microendoscopy. Nat Med 2011; 17:223-8; PMID:21240263; http://dx.doi.org/10.1038/nm.2292
32. Yoshihara Y, De Roo M, Muller D. Dendritic spine formation and stabilization. Curr Opin Neurobiol 2009; 19:146-53; PMID:19523814; http://dx.doi.org/10.1016/j.conb.2009.05.013
33. Zuo Y, Lin A, Chang P, Gan W-B. Development of long-term dendritic spine stability in diverse regions of cerebral cortex. Neuron 2005; 46:181-9; PMID:15848798; http://dx.doi.org/10.1016/j.neuron.2005.04.001
34. Grutzendler J, Kasthuri N, Gan W-B. Long-term dendritic spine stability in the adult cortex. Nature 2002; 420:812-6; PMID:12490949; http://dx.doi.org/10.1038/nature01276
35. Lee W-CA, Chen JL, Huang H, Leslie JH, Amitai Y, So PT, Nedivi E. A dynamic zone defines interneuron remodeling in the adult neocortex. Proc Natl Acad Sci U S A 2008; 105:19968-73; PMID:19066223; http://dx.doi.org/10.1073/pnas.0810149105
36. Brown CE, Aminoltejari K, Erb H, Winship IR, Murphy TH. In vivo voltage-sensitive dye imaging in adult mice reveals that somatosensory maps lost to stroke are replaced over weeks by new structural and functional circuits with prolonged modes of activation within both the peri-infarct zone and distant sites. J Neurosci 2009; 29:1719-34; PMID:19211879; http://dx.doi.org/10.1523/JNEUROSCI.4249-08.2009
37. Brown CE, Li P, Boyd JD, Delaney KR, Murphy TH. Extensive turnover of dendritic spines and vascular remodeling in cortical tissues recovering from stroke. J Neurosci 2007; 27:4101-9; PMID:17428988; http://dx.doi.org/10.1523/JNEUROSCI.4295-06.2007
38. Keck T, Mrsic-Flogel TD, Vaz Afonso M, Eysel UT, Bonhoeffer T, Hübener M. Massive restructuring of neuronal circuits during functional reorganization of adult visual cortex. Nat Neurosci 2008; 11:1162-7; PMID:18758460; http://dx.doi.org/10.1038/nn.2181
39. Feng G, Mellor RH, Bernstein M, Keller-Peck C, Nguyen QT, Wallace M, Nerbonne JM, Lichtman JW, Sanes JR. Imaging neuronal subsets in transgenic mice expressing multiple spectral variants of GFP. Neuron 2000; 28:41-51; PMID:11086982; http://dx.doi.org/10.1016/S0896-6273(00)00084-2
40. Isshiki M, Okabe S. Evaluation of cranial window types for in vivo two-photon imaging of brain microstructures. Microsc Oxf Engl 2013
41. Ransohoff RM, Perry VH. Microglial physiology: unique stimuli, specialized responses. Annu Rev Immunol 2009; 27:119-45; PMID:19302036; http://dx.doi.org/10.1146/annurev.immunol.021908.132528
42. Burda JE, Sofroniew MV. Reactive gliosis and the multicellular response to CNS damage and disease. Neuron 2014; 81:229-48; PMID:24462092; http://dx.doi.org/10.1016/j.neuron.2013.12.034
43. Kettenmann H, Hanisch U-K, Noda M, Verkhratsky A. Physiology of microglia. Physiol Rev 2011; 91:461-553; PMID:21527731; http://dx.doi.org/10.1152/physrev.00011.2010
44. Hauss-Wegrzyniak B, Lynch MA, Vraniak PD, Wenk GL. Chronic brain inflammation results in cell loss in the entorhinal cortex and impaired LTP in perforant path-granule cell synapses. Exp Neurol 2002; 176:336-41; PMID:12359175; http://dx.doi.org/10.1006/exnr.2002.7966
45. Burgold S, Bittner T, Dorostkar MM, Kieser D, Fuhrmann M, Mitteregger G, Kretzschmar H, Schmidt B, Herms J. In vivo multiphoton imaging reveals gradual growth of newborn amyloid plaques over weeks. Acta Neuropathol 2011; 121:327-35; PMID:21136067; http://dx.doi.org/10.1007/s00401-010-0787-6
46. Norton WT, Aquino DA, Hozumi I, Chiu F-C, Brosnan CF. Quantitative aspects of reactive gliosis: a review. Neurochem Res 1992; 17:877-85; PMID:1407275; http://dx.doi.org/10.1007/BF00993263
47. Silver J, Miller JH. Regeneration beyond the glial scar. Nat Rev Neurosci 2004; 5:146-56; PMID:14735117; http://dx.doi.org/10.1038/nrn1326
48. Potter KA, Buck AC, Self WK, Capadona JR. Stab injury and device implantation within the brain results in inversely multiphasic neuroinflammatory and neurodegenerative responses. J Neural Eng 2012; 9:046020; PMID:22832283; http://dx.doi.org/10.1088/1741-2560/9/4/046020
49. Pekny M, Nilsson M. Astrocyte activation and reactive gliosis. Glia 2005; 50:427-34; PMID:15846805; http://dx.doi.org/10.1002/glia.20207
50. Eliasson C, Sahlgren C, Berthold C-H, Stakeberg J, Celis JE, Betsholtz C, Eriksson JE, Pekny M. Intermediate filament protein partnership in astrocytes. J Biol Chem 1999; 274:23996-4006; PMID:10446168; http://dx.doi.org/10.1074/jbc.274.34.23996
51. Pekny M, Wilhelmsson U, Pekna M. The dual role of astrocyte activation and reactive gliosis. Neurosci Lett [Internet] [cited 2014 Feb 25]; Available from: http://www.sciencedirect.com/science/article/pii/S0304394014000081
52. Wilhelmsson U, Li L, Pekna M, Berthold C-H, Blom S, Eliasson C, Renner O, Bushong E, Ellisman M, Morgan TE, et al. Absence of glial fibrillary acidic protein and vimentin prevents hypertrophy of astrocytic processes and improves post-traumatic regeneration. J Neurosci 2004; 24:5016-21; PMID:15163694; http://dx.doi.org/10.1523/JNEUROSCI.0820-04.2004
53. Eng LF. Glial fibrillary acidic protein (GFAP): the major protein of glial intermediate filaments in differentiated astrocytes. J Neuroimmunol 1985; 8:203-14; PMID:2409105; http://dx.doi.org/10.1016/S0165-5728(85)80063-1
54. Seifert G, Schilling K, Steinhäuser C. Astrocyte dysfunction in neurological disorders: a molecular perspective. Nat Rev Neurosci 2006; 7:194-206; PMID:16495941; http://dx.doi.org/10.1038/nrn1870
55. Zhuo L, Sun B, Zhang CL, Fine A, Chiu SY, Messing A. Live astrocytes visualized by green fluorescent protein in transgenic mice. Dev Biol 1997; 187:36-42; PMID:9224672; http://dx.doi.org/10.1006/dbio.1997.8601
56. Kozlowski C, Weimer RM. An automated method to quantify microglia morphology and application to monitor activation state longitudinally in vivo. PLoS One 2012; 7:e31814; PMID:22457705; http://dx.doi.org/10.1371/journal.pone.0031814

57. Beynon SB, Walker FR. Microglial activation in the injured and healthy brain: what are we really talking about? Practical and theoretical issues associated with the measurement of changes in microglial morphology. Neuroscience 2012; 225:162-71; PMID:22824429; http://dx.doi.org/10.1016/j.neuroscience.2012.07.029
58. Mizutani M, Pino PA, Saederup N, Charo IF, Ransohoff RM, Cardona AE. The fractalkine receptor but not CCR2 is present on microglia from embryonic development throughout adulthood. J Immunol 2012; 188:29-36; PMID:22079990; http://dx.doi.org/10.4049/jimmunol.1100421
59. Haynes SE, Hollopeter G, Yang G, Kurpius D, Dailey ME, Gan W-B, Julius D. The P2Y12 receptor regulates microglial activation by extracellular nucleotides. Nat Neurosci 2006; 9:1512-9; PMID:17115040; http://dx.doi.org/10.1038/nn1805
60. Davalos D, Ryu JK, Merlini M, Baeten KM, Le Moan N, Petersen MA, Deerinck TJ, Smirnoff DS, Bedard C, Hakozaki H, et al. Fibrinogen-induced perivascular microglial clustering is required for the development of axonal damage in neuroinflammation. Nat Commun 2012; 3:1227; PMID:23187627; http://dx.doi.org/10.1038/ncomms2230
61. Hinwood M, Tynan RJ, Charnley JL, Beynon SB, Day TA, Walker FR. Chronic stress induced remodeling of the prefrontal cortex: structural re-organization of microglia and the inhibitory effect of minocycline. Cereb Cortex 2013; 23:1784-97; PMID:22710611; http://dx.doi.org/10.1093/cercor/bhs151
62. Graeber MB, Streit WJ, Kiefer R, Schoen SW, Kreutzberg GW. New expression of myelomonocytic antigens by microglia and perivascular cells following lethal motor neuron injury. J Neuroimmunol 1990; 27:121-32; PMID:2332482; http://dx.doi.org/10.1016/0165-5728(90)90061-Q
63. Kim Y-J, Hwang S-Y, Oh E-S, Oh S, Han I-O. IL-1β, an immediate early protein secreted by activated microglia, induces iNOS/NO in C6 astrocytoma cells through p38 MAPK and NF-kappaB pathways. J Neurosci Res 2006; 84:1037-46; PMID:16881054; http://dx.doi.org/10.1002/jnr.21011
64. Burguillos MA, Deierborg T, Kavanagh E, Persson A, Hajji N, Garcia-Quintanilla A, Cano J, Brundin P, Englund E, Venero JL, et al. Caspase signalling controls microglia activation and neurotoxicity. Nature 2011; 472:319-24; PMID:21389984; http://dx.doi.org/10.1038/nature09788
65. Frautschy SA, Yang F, Irrizarry M, Hyman B, Saido TC, Hsiao K, Cole GM. Microglial response to amyloid plaques in APPsw transgenic mice. Am J Pathol 1998; 152:307-17; PMID:9422548
66. Bolmont T, Haiss F, Eicke D, Radde R, Mathis CA, Klunk WE, Kohsaka S, Jucker M, Calhoun ME. Dynamics of the microglial/amyloid interaction indicate a role in plaque maintenance. J Neurosci 2008; 28:4283-92; PMID:18417708; http://dx.doi.org/10.1523/JNEUROSCI.4814-07.2008
67. Cruz-Martín A, Crespo M, Portera-Cailliau C. Delayed stabilization of dendritic spines in fragile X mice. J Neurosci 2010; 30:7793-803; PMID:20534828; http://dx.doi.org/10.1523/JNEUROSCI.0577-10.2010
68. Golshani P, Gonçalves JT, Khoshkhoo S, Mostany R, Smirnakis S, Portera-Cailliau C. Internally mediated developmental desynchronization of neocortical network activity. J Neurosci 2009; 29:10890-9; PMID:19726647; http://dx.doi.org/10.1523/JNEUROSCI.2012-09.2009
69. Myers JT, Barkauskas DS, Huang AY. Dynamic Imaging of Marrow-Resident Granulocytes Interacting with Human Mesenchymal Stem Cells upon Systemic Lipopolysaccharide Challenge. Stem Cells Int 2013; 2013:656839; PMID:23606861; http://dx.doi.org/10.1155/2013/656839
70. Kerschensteiner M, Schwab ME, Lichtman JW, Misgeld T. In vivo imaging of axonal degeneration and regeneration in the injured spinal cord. Nat Med 2005; 11:572-7; PMID:15821747; http://dx.doi.org/10.1038/nm1229
71. Misgeld T, Nikic I, Kerschensteiner M. In vivo imaging of single axons in the mouse spinal cord. Nat Protoc 2007; 2:263-8; PMID:17406584; http://dx.doi.org/10.1038/nprot.2007.24
72. Steffens H, Nadrigny F, Kirchhoff F. In vivo two-photon imaging of neurons and glia in the mouse spinal cord. Cold Spring Harb Protoc 2012; 2012:pii: pdb.prot072264; PMID:23209139; http://dx.doi.org/10.1101/pdb.prot072264
73. Farrar MJ, Bernstein IM, Schlafer DH, Cleland TA, Fetcho JR, Schaffer CB. Chronic in vivo imaging in the mouse spinal cord using an implanted chamber. Nat Methods 2012; 9:297-302; PMID:22266542; http://dx.doi.org/10.1038/nmeth.1856
74. Davalos D, Lee JK, Smith WB, Brinkman B, Ellisman MH, Zheng B, Akassoglou K. Stable in vivo imaging of densely populated glia, axons and blood vessels in the mouse spinal cord using two-photon microscopy. J Neurosci Methods 2008; 169:1-7; PMID:18192022; http://dx.doi.org/10.1016/j.jneumeth.2007.11.011
75. Johannssen HC, Helmchen F. Two-photon imaging of spinal cord cellular networks. Exp Neurol 2013; 242:18-26; PMID:22849822; http://dx.doi.org/10.1016/j.expneurol.2012.07.014
76. Evans TA, Barkauskas DS, Myers JT, Hare EG, You JQ, Ransohoff RM, Huang AY, Silver J. High-resolution intravital imaging reveals that blood-derived macrophages but not resident microglia facilitate secondary axonal dieback in traumatic spinal cord injury. Exp Neurol 2014; 254:109-20; PMID:24468477; http://dx.doi.org/10.1016/j.expneurol.2014.01.013
77. Stromnes IM, Goverman JM. Active induction of experimental allergic encephalomyelitis. Nat Protoc 2006; 1:1810-9; PMID:17487163; http://dx.doi.org/10.1038/nprot.2006.285
78. Toriumi H, Shimizu T, Shibata M, Unekawa M, Tomita Y, Tomita M, Suzuki N. Developmental and circulatory profile of the diploic veins. Microvasc Res 2011; 81:97-102; PMID:21093458; http://dx.doi.org/10.1016/j.mvr.2010.11.004
79. Holtmaat A, Wilbrecht L, Knott GW, Welker E, Svoboda K. Experience-dependent and cell-type-specific spine growth in the neocortex. Nature 2006; 441:979-83; PMID:16791195; http://dx.doi.org/10.1038/nature04783
80. Tsai J, Grutzendler J, Duff K, Gan W-B. Fibrillar amyloid deposition leads to local synaptic abnormalities and breakage of neuronal branches. Nat Neurosci 2004; 7:1181-3; PMID:15475950; http://dx.doi.org/10.1038/nn1335